PAPER

Check for updates

Sulfur-containing bimetallic metal organic frameworks with multi-fold helix as anode of lithium ion batteries†

Meng-Ting Li,‡[a] Ning Kong,‡[a] Ya-Qian Lan [ID] *[b] and Zhong-Min Su [ID] *[a]

We utilise the dual synthesis strategy in terms of bimetallic inorganic building blocks and sulfur containing organic ligand. A novel sulfur-containing bimetallic metal organic framework (Fe_2Co-TPDC) with two types of 4-fold meso-helical structures has been successfully synthesized. Benefitting from the uniform distribution of active sulfur sites and the structural stability of the mixed-metallic method, Fe_2Co-TPDC can efficiently prevent a shuttle behavior of sulfur and endow a commendable specific capacity. As far as we know, this is the first time that a sulfur-containing bimetallic crystalline MOF with helical structure and prominent specific capacity and remarkable cycling stability has served as an electrode material for LIBs.

Introduction

The exploitation of renewable green energy sources and storage devices is imperative due to the increasing consumption of non-renewable resources.[1-3] As an up-and-coming power source, lithium-ion batteries (LIBs) have been widely considered for multitudinous electronic equipment, on account of having high storage capacities and excellent cycle performance.[4-8] Nonetheless, there are two main obstacles, including specific capacity and safety problems, in the development of the LIBs electrode materials:[9,10] conventional graphite materials have a deficient theoretical specific capacity of 372 mA h g^{-1}, while silicon-based materials suffer from an exaggerated volume expansion (~300%) upon cycling, resulting in limited rate performances and pulverization of the electrodes.[11-13] As a consequence, calling on the masses for developing fungible LIBs electrode materials makes a lot of sense.

In the LIBs electrode materials, recently, several instances are available for crystalline metal–organic frameworks (MOFs) acting as an anode/cathode based on topotactic ion insertion and nontopotactic ion insertion.[14-16] MOFs are a new type of crystalline hybrids with a kaleidoscopic configuration, long-range ordered arrangement of metal nodes and organic linkers, sizable surface area and multi-functions that provide a novel field for host–guest interactions.[17-20] Their high stability at increased temperatures is advantageous for their use under harsh conditions.[21] In 2007, Tarascon *et al.* reported MIL-53 (Fe) as a cathode material for LIBs for the first time.[22] Since then, more and more stable crystalline MOFs and MOF derivatives are constantly being developed.[23-27] What is less explored, however, is the development of bimetallic MOFs, especially in the field of LIBs.[28-30] Benefiting from the synergistic effect of the mixed-metallic method, bimetallic MOFs can offer an additional degree of structural stability and endow LIBs with better electrode performances.[31-33] Unfortunately, the synthesis of bimetallic MOFs is very challenging because of the unpredictable *in situ* formation of subunit building blocks during 'one-pot' synthetic procedures.[34,35] To address these problems, Zhou *et al.* obtained a great deal of bimetallic MOFs by utilizing preformed inorganic building blocks [Fe_2M (μ_3-O)($CH_3COO)_6$] (M = $Fe^{2+,3+}$, Co^{2+} *etc.*).[36] It is expected that bimetallic MOFs can not only offer structural complexity through a 'one-pot' synthetic route, but also help buffer the volume expansion/contraction upon cycling.

In addition, for the sake of higher specific capacity, sulfur and metal sulfides used to be the center of attention as promising electrodes for LIBs mainly due to the active sulfur element delivering a considerable theoretical capacity of 1675 mA h g^{-1}.[37,38] In contrast, the sulfur containing materials are always subjected to severe capacity fading and poor cyclability, which are mainly attributed to the large volume change and formation of polysulfides Li_2S_x (2 < x < 8) upon cycling.[39,40] The polysulfides are the intermediates of the

[a]*Institute of Functional Material Chemistry, National & Local United Engineering Laboratory for Power Batteries, Northeast Normal University, Changchun, 130024 Jilin, People's Republic of China. E-mail: zmsu@nenu.edu.cn*
[b]*School of Chemistry and Materials Science, Nanjing Normal University, Nanjing, 210023, People's Republic of China. E-mail: yqlan@njnu.edu.cn*
†Electronic supplementary information (ESI) available: Materials and measurements, experimental, figures and tables. CCDC 1814820. For ESI and crystallographic data in CIF or other electronic format see DOI: 10.1039/c8dt00095f
‡These authors contributed equally to this work.

electrochemical reactions during the Li+ insertion/extraction process, which can facilely dissolve into the electrolyte or transfer to the surface of the electrode, leading to a shuttle behavior and rapid capacity fading. As a result of this and in conjunction with the heterogeneous diffusion of a traditional sulfur containing technique, there has been an increased demand for the anchoring of sulfur containing organic ligand onto MOFs. By understanding this, the long-range ordered arrangement of pore structures can ensure the uniform distribution of active sulfur sites, which strikingly prevents the loss of sulfur. It is anticipated that the strategy of combining bimetallic centers with sulfur-containing ligands can synergistically facilitate the specific capacity and cycling stability of LIBs.

In this article, we aim to focus on two intriguing characteristics of bimetallic MOFs. One is the dual synthesis strategy in terms of bimetallic inorganic building blocks ($[Fe_2Co(COO)_6]$) and sulfur containing organic ligand (thiophene-2,5-dicarboxylic acid (H_2TPDC)), and the other is the ability of applying it to LIBs. Fortunately, a novel sulfur-containing bimetallic MOF has been successfully synthesized, namely $[Fe_2Co(TPDC)_3(C_3H_6NO)_3]$ (abbreviated as Fe$_2$Co-TPDC). Unexpectedly, the 3D porous architecture of Fe$_2$Co-TPDC contains two kinds of multi-fold helixes, which are considered as favourable factors for structural stability and electrochemical performances. To our knowledge, this is the first time that a sulfur-containing bimetallic crystalline MOF with helical structure has served as an electrode material for LIBs and displayed commendable specific capacity and cycling stability.

Experimental

Preparation of $[Fe_2Co(\mu_3\text{-}O)(CH_3COO)_6]$

$[Fe_2Co(\mu_3\text{-}O)(CH_3COO)_6]$ was isolated using a previously reported method.[41] $Fe(NO_3)_3 \cdot 9H_2O$ 8 g (0.02 mol) and $Co(NO_3)_2 \cdot 6H_2O$ 29 g (0.1 mol) were dissolved in 70 ml distilled water for further use (solution A). $CH_3COONa \cdot 3H_2O$ (42 g, 0.31 mol) was dissolved in 70 ml distilled water for further use (solution B). Solution B was slowly added to solution A at room temperature with continuous stirring. Stirring was continued for a further 10 min even after a precipitate was formed. The precipitate was collected by centrifugation and washed with distilled water and ethanol. Then, the red sample was dried at room temperature, yielding $[Fe_2Co(\mu_3\text{-}O)(CH_3COO)_6]$.

Preparation of Fe$_2$Co-TPDC

Fe$_2$Co-TPDC was synthesized by using a solvothermal method. A mixture of $[Fe_2Co(\mu_3\text{-}O)(CH_3COO)_6]$ (0.030 g) and H_2TPDC (0.017 g) was dispersed in 5 mL DMF. Then, 0.25 ml acetic acid was added to the mixture and the mixture was transferred to a Teflon-lined reactor and heated at 150 °C for 48 h. The dark red blocks crystals were collected at ambient temperature. Yield: 60% based on Fe. Anal. calc for $C_{27}H_{24}N_3O_{15}S_3Fe_2Co$: C, 36.14; H, 2.7; O, 26.75; N, 4.68; S, 10.72. Found: C, 36.10; H,

2.75; O, 26.71; N, 4.65; S, 10.76. For details of Fe$_2$Co-TPDC please see Table S1 in the ESI.†

Materials and measurements

Powder X-ray diffraction (PXRD) patterns, FT-IR spectra, thermogravimetric analysis (TGA) and elemental analyses were performed on a Siemens D5005 diffractometer (Cu-Kα (λ = 1.5418 Å) radiation), Alpha Centaurt FT/IR spectrophotometer (KBr pellets), PerkinElmer TG-7 analyzer and PerkinElmer 240C elemental analyzer, respectively. Inductively coupled plasma (ICP) was performed on an inductively coupled plasma source mass spectrometer (ICP-MS, Agilent 7700x).

X-ray crystallographic measurements

A Bruker SMART-CCD diffractometer with monochromatic Mo-Kα radiation (λ = 0.71069 Å) was used for collecting the crystallographic data of Fe$_2$Co-TPDC at 293 K. Absorption corrections were applied using a multiscan technique and conducted using the SADABS program.[42] To solve and refine the structures of the title compounds, we employed the direct method and the full matrix least-squares with the *SHELXTL* program.[43] We used the anisotropic operation to refine all the atoms except for hydrogen atoms.

Battery analyses

In this study, we used a half-cell to investigate the electrochemical performance of Fe$_2$Co-TPDC. The half-cell was assembled with Fe$_2$Co-TPDC as the working electrode and Li metal as the counter electrode. So, the Fe$_2$Co-TPDC was the cathode and Li metal, the anode. The cathode was obtained by mixing Fe$_2$Co-TPDC, Super-P carbon, and poly(vinylidene fluoride) according to the weight ratio 70 : 20 : 10. The purpose of extra N-methyl-2-pyrrolidinone (NMP) was to make the mixture into a paste with appropriate viscosity. Then, the paste was coated on a pure Cu foil mildly and vacuum dried at 50 °C for 24 h. The cathode loading mass on each electrode disk was about 2 mg cm^{-2}. A button cell was assembled with the working electrode, Li counter electrode, and 1.0 M LiPF$_6$ in ethylene carbonate (EC)/diethyl carbonate (DEC) (1 : 1 v/v) as the electrolyte. The electrochemical performance of Fe$_2$Co-TPDC cathode, for instance, by circulation measurements, cyclic voltammetry (CV) and electrochemical impedance spectroscopy (EIS) was tested on a LAND CT2001A instrument (Wuhan, China) and an electrochemical workstation (Princeton Applied Research, Germany) at room temperature.

Results and discussion

The FT-IR spectra of Fe$_2$Co-TPDC was confirmed, see Fig. S1.† TGA of Fe$_2$Co-TPDC indicated that the weight loss before 300 °C was solvent molecules. The whole framework of Fe$_2$Co-TPDC completely collapsed after 400 °C (Fig. S2†). The experimental PXRD pattern of Fe$_2$Co-TPDC agreed with the simulated patterns, which indicated the pure phase of Fe$_2$Co-TPDC (Fig. S3†). Single-crystal data revealed that Fe$_2$Co-TPDC crystal-

lizes in the monoclinic space group $P2_1/c$. Generally, $M_3(\mu_3\text{-O})(COO)_6$ (M = Fe, *etc.*) is a usual inorganic subunit building block in MOFs system.[44] Hence, we used $[Fe_2Co(\mu_3\text{-O})(CH_3COO)_6]$ as the precursor to construct bimetallic MOF. However, single-crystal data of $Fe_2Co\text{-TPDC}$ revealed that $[Fe_2Co(\mu_3\text{-O})(CH_3COO)_6]$ repeatedly split and assembled even though Fe^{3+} and $\mu_3\text{-O}^{2-}$ possessed strong electrostatic interactions. The fissile mechanism of building blocks under solvothermal condition is still unclear; we speculate that the Co^{2+} ion escaped from the original cluster, and recombined with two Fe^{3+} ions to form a lineal cluster eventually (Fig. S4†). Inductively coupled plasma (ICP) of $Fe_2Co\text{-TPDC}$ indicated that the weight fraction of Fe^{3+} ions was 13.92 and Co^{2+} ions was 5.11, corresponding to the ratio of Fe : Co = 2 : 1. The reborn $[Fe_2Co(COO)_6]$ cluster (abbreviated as $[Fe_2Co]$) itself possessed six carboxylate arms. The adjacent $[Fe_2Co]$ clusters were linked to each other end to end, which constituted a 1D inorganic metal chain (Fig. S5†). One single Fe_2Co cluster coordinated with seven $TPDC^{2-}$ ligands (Fe–O, 1.959(5)–2.043(5) Å, Table S2†) to extend a $[Fe_2Co(TPDC)_6]$ unit. Bond-valence calculation indicated that the oxidation state of Fe cations is +3 and Co cations is +2.[45,46]

The framework contains two different kinds of multi-fold helixes with different diameters along the *b* axis. Type-I 4-fold meso-helix, which is the helical channel with a large size of 14.1 × 14.8 Å, is composed of two left-handed helixes with the thread of $\{[Fe_2Co]\text{-}[Fe_2Co]\text{-TPDC-}[Fe_2Co]\text{-TPDC-}[Fe_2Co]\text{-TPDC}\}$ and two right-handed helixes in the same route (Fig. 1). Two independent left-handed helixes are arranged in the double left-handed helix along the identical axis and same is the case with the double right-handed helix. These double left- and right-handed helixes with a thread pitch of 19.5 Å fabricate into a Type-I 4-fold meso-helix by partially sharing themselves (Fig. 2). The helical channel with a small size of 10.7 × 16.2 Å, namely Type-II 4-fold meso-helix, is formed by left- and right-handed helixes in a similar way (Fig. S6†). Two independent left-handed helixes following the principle of $\{[Fe_2Co]\text{-}[Fe_2Co]\text{-TPDC-}[Fe_2Co]\text{-TPDC-}[Fe_2Co]\text{-TPDC}\}$ are formed, which look exactly like the Type-I 4-fold meso-helix. In contrast, some of the asymmetric $[Fe_2Co]$ clusters in the helical route just contribute part of themselves, combining with the variety of coordination patterns of each ligand and that induces the imparity of two types of 4-fold meso-helixes. Type-I and Type-II 4-fold meso-helix generate an infinite 3D porous framework by partially sharing building blocks. To simplify the complex structure of $Fe_2Co\text{-TPDC}$, the $[Fe_2Co]$ cluster can be seen as eight-connected nodes based on the topology, and the $TPDC^{2-}$ ligand will not be considered as a node due to its double coordination form. The whole network can resemble a single-modal 8-net with a point symbol of $\{4^{24}\cdot6^4\}$ (Fig. S7†). There is 1599.5 Å^3 potential solvent area volume (44.5% per unit cell) in $Fe_2Co\text{-TPDC}$ calculated by the PLATON routine.[47]

The electrochemical properties of $Fe_2Co\text{-TPDC}$, which were triggered by the fascinating dual synthesis strategy, have been evaluated by using $Fe_2Co\text{-TPDC}$ as LIBs cathode materials. Cyclic voltammograms (CV) of $Fe_2Co\text{-TPDC}$ were obtained over
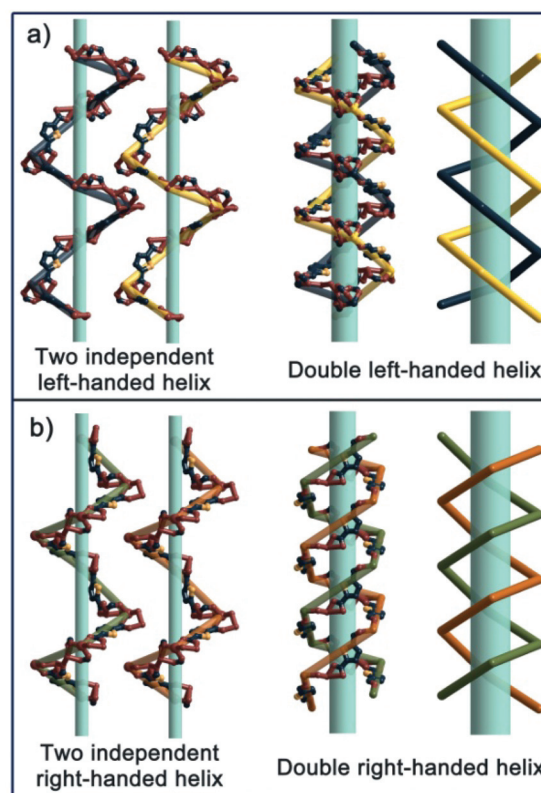

Fig. 1 Ball/stick diagrams of (a) the single left-handed helix and double left-handed helix; (b) single right-handed helix and double right-handed helix in Type-I 4-fold meso-helix of $Fe_2Co\text{-TPDC}$. All of the hydrogen atoms are omitted for clarity.
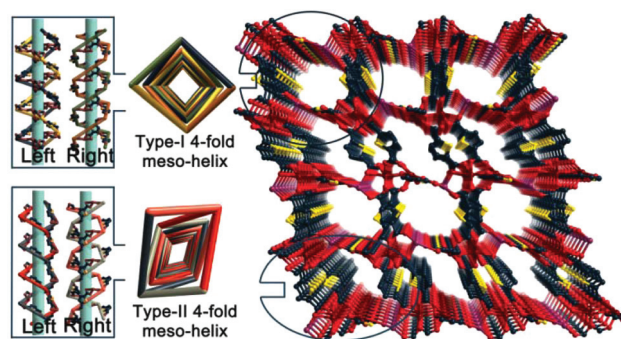

Fig. 2 Ball/stick diagrams of Type-I and Type-II 4-fold meso-helix of $Fe_2Co\text{-TPDC}$, and the whole 3D $Fe_2Co\text{-TPDC}$ framework. All of the hydrogen atoms are omitted for clarity.

the range of 0.01–3 V, with a scan rate of 0.1 mV s^{-1} (Fig. S8†). At the first CV cycle, the fabric of the solid electrolyte interphase (SEI) films caused an irreversible reduction peak around 0.7 V, which is a normal phenomenon in LIBs.[48] This peak slightly receded at the second cycle, and there was almost no more change in the third cycle. This indicated a sluggish forming process of SEI films. The Li$^+$ insertion procedure induced a reduction peak at 0.01–0.2 V. In addition, we used electrochemical impedance spectroscopy (EIS) to study the

dynamics performance of Fe$_2$Co-TPDC (Fig. S9†). As a rule, the resistance R value is determined by solid electrolyte interface resistance (high-frequency semicircle) and the interfacial reactions for Li$^+$ migration resistance at the surface of the electrode (semicircle at mid-frequency). The R values were 29 and 21 Ω for Fe$_2$Co-TPDC before cycling and after the 100th discharge–charge process, respectively. This indicates that the sulfur-containing bimetallic organic framework can offer a passageway for rapid Li$^+$ ions transportation, which promotes the electrochemical performance. Furthermore, we speculate that the possible mechanism for Li storage may be expressed as the intercalation of Li$^+$ into the sulfur-containing ligand (carboxylic group and thiophene ring). As shown in Fig. S10,† there are 8 possible Li+ insertion sites, one Li$^+$ in each carboxylic group, two Li$^+$ in the sulfur site and four Li$^+$ in the rest of the thiophene ring.

To test our hypothesis that the sulfur-containing MOF undergoing a dual synthesis strategy can efficaciously enhance the battery performance, commercial graphite also has been investigated as a reference. The first discharge capacities of the Fe$_2$Co-TPDC and graphite are 1973 mA h g^{-1} and 624 mA h g^{-1}, respectively (Fig. 3 and S11†), and the capacities drop to 930 mA h g^{-1} and 409 mA h g^{-1} in the next cycle. The dramatic reduction in capacity after the first cycle is caused by the formation of the SEI films.

As shown in Fig. 4 and S12,† the cycling capacity of the Fe$_2$Co-TPDC cathode remains stable above 900 mA h g^{-1} for 100 cycles at the current density 0.1C (0.1C = 100 mA cm^{-2}). The discharge capacity of Fe$_2$Co-TPDC exhibits an upswing from 746 mA h g^{-1} to 991 mA h g^{-1} at 0.1C before 20–30 cycles. On one hand, the activation phenomenon may be attributed to the sluggish forming process of SEI films. On the other hand, we suspect that Li$^+$ has hardly any access to the interior of the helical channel at the beginning due to the nano-pore sizes of crystalline Fe$_2$Co-TPDC materials. It needs some time for Li$^+$ to completely reach the sulfur active sites. In comparison, the capacity of graphite shows a decent stable capacity at *ca.* 300 mA h g^{-1}.

The charge–discharge capacities of Fe$_2$Co-TPDC at a current density 0.2C, 1C and 2C are *ca.* 800 mA h g^{-1}, 500 mA h g^{-1} and 400 mA h g^{-1}, respectively (Fig. 5). It indicates that Fe$_2$Co-

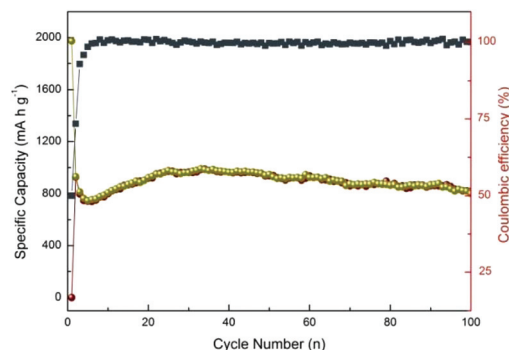**Fig. 4** The charge−discharge capacity and the Coulombic efficiency of Fe$_2$Co-TPDC during 100 cycles at a current density 0.1C (0.1C = 100 mA cm^{-2}).
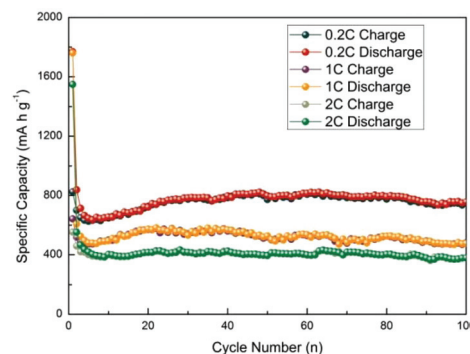

Fig. 5 The charge−discharge capacity of Fe$_2$Co-TPDC at a current density 0.2C, 1C and 2C.

TPDC is qualified for the working environment with a high current density. Obviously, both the capacity retention and cycling stability of Fe$_2$Co-TPDC have a huge advantage in comparison with graphite during the cycling process.

Normally, cycling and rate performance of LIBs are the assessment criteria for commercial applications. It is noteworthy that Fe$_2$Co-TPDC displays favorable rate performance and cycling stability at current densities from 0.1C to 1C (Fig. 6). The reversible capacities of Fe$_2$Co-TPDC at 0.1C are 868 mA h g^{-1} and 898 mA h g^{-1}. Even at 1C, Fe$_2$Co-TPDC can retain capacities of 667 mA h g^{-1} and 662 mA h g^{-1}. When the current density is reset back to 0.1C after 40 cycles, the specific capacities of Fe$_2$Co-TPDC almost recover to the original state. The capacity of graphite is much lower than that of Fe$_2$Co-TPDC at each current density (Fig. S13†). These results indicate that the sulfur-containing bimetallic Fe$_2$Co-TPDC framework with helical structure promotes the electrochemical performance of LIBs.

We speculate that the coordination angle of H$_2$TPDC and asymmetric [Fe$_2$Co] clusters dominates the successful synthesis and superior performance of Fe$_2$Co-TPDC (Fig. 7). Above all, the native coordination angle of 151.7° within sulfur-containing H$_2$TPDC ligand can induce a turbinate formation instead of a linear pattern with metal clusters during the sub-
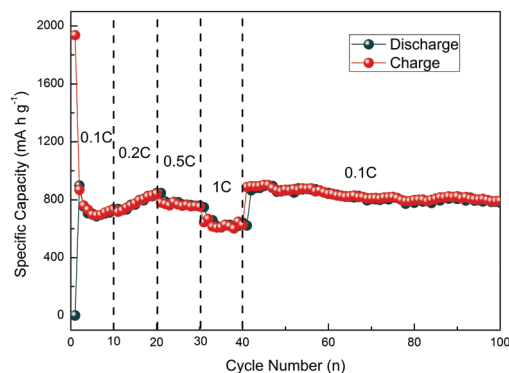

Fig. 3 The charge−discharge curves of Fe$_2$Co-TPDC before 50 cycles at a current density of 0.1C (0.1C = 100 mA cm^{-2}).

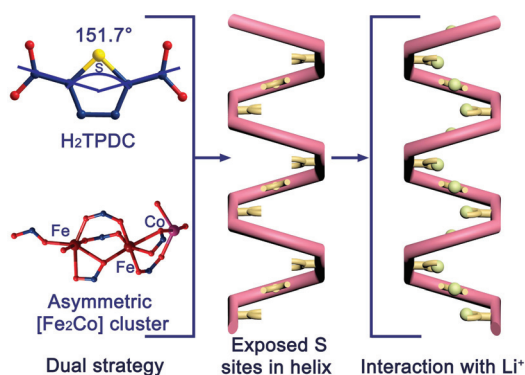**Fig. 6** Rate performance of Fe$_2$Co-TPDC at current densities of 0.1C to 1C.

Fig. 7 Representations of the dual synthesis strategy for the sulfur-containing helical structure. The sulfur atoms can be exposed into the inner cavity of helical channels, which increases the interaction of sulfur and Li$^+$ during the discharge/charge process.

stitution reaction and deprotonation process. The D_{3h} [Fe$_2$Co (μ_3-O)(CH$_3$COO)$_6$] clusters as the starting material break and reform to the asymmetric [Fe$_2$Co] clusters that lead to a brand new metal species with a more complicated coordinating space. As a consequence, two types of 4-fold meso-helixes have been created in the sulfur-containing bimetallic Fe$_2$Co-TPDC framework. In addition, a major advantage is that all the sulfur atoms have been exposed into the inner cavity of the helical channels, which means the Fe$_2$Co-TPDC framework can not only prevent a shuttle behavior and rapid capacity fading of sulfur, but also endow a fast Li$^+$ intercalation/deintercalation kinetics.

Conclusions

In summary, by utilizing the dual synthesis strategy in terms of bimetallic inorganic building blocks and sulfur-containing organic ligand, a novel sulfur-containing bimetallic Fe$_2$Co-TPDC with two types of 4-fold meso-helical structures has been successfully synthesized. Notably, Fe$_2$Co-TPDC is capable of acting as a cathode due to structural stability and electro-

chemical performances. Benefitting from the uniform distribution of active sulfur sites and the structural stability of the mixed-metallic method, the Fe$_2$Co-TPDC framework can not only prevent a shuttle behavior and rapid capacity fading of sulfur, but also endow a fast Li$^+$ intercalation/deintercalation kinetics. As far as we know, this is the first time that a sulfur-containing bimetallic crystalline MOF with a helical structure has served as a cathode and displayed commendable specific capacity and cycling stability.

Conflicts of interest

There are no conflicts to declare.

Acknowledgements

Notes and references

1 M. Armand and J. M. Tarascon, *Nature*, 2008, **451**, 652–657.
2 Z. Yang, J. Zhang, M. C. W. Kintner-Meyer, X. Lu, D. Choi, J. P. Lemmon and J. Liu, *Chem. Rev.*, 2011, **111**, 3577–3613.
3 Y. Zhong, M. Yang, X. Zhou and Z. Zhou, *Mater. Horiz.*, 2015, **2**, 553–566.
4 T. Wei, M. Zhang, P. Wu, Y. J. Tang, S. L. Li, F. C. Shen, X. L. Wang, X. P. Zhou and Y. Q. Lan, *Nano Energy*, 2017, **34**, 205–214.
5 T. Yamada, K. Shiraishi, H. Kitagawa and N. Kimizuka, *Chem. Commun.*, 2017, **53**, 8215–8218.
6 J. R. Miller, R. A. Outlaw and B. C. Holloway, *Science*, 2010, **329**, 1637–1639.
7 F. Wang, H. Zhuo, X. Han, W. Chen and D. Sun, *J. Mater. Chem. A*, 2017, **5**, 22964–22969.
8 W. Huang, S. Li, X. Y. Cao, C. Y. Hou, Z. Zhang, J. K. Feng, L. J. Ci, P. C. Si and Q. J. Chi, *ACS Sustainable Chem. Eng.*, 2017, **5**, 5039–5048.
9 V. Palomares, P. Serras, I. Villaluenga, K. B. Hueso, J. Carretero-González and T. Rojo, *Energy Environ. Sci.*, 2012, **5**, 5884–5901.
10 M. D. Slater, D. Kim, E. Lee and C. S. Johnson, *Adv. Funct. Mater.*, 2013, **23**, 947–958.
11 J. Ji, H. Ji, L. L. Zhang, X. Zhao, X. Bai, X. Fan, F. Zhang and R. S. Ruoff, *Adv. Mater.*, 2013, **25**, 4673–4677.
12 L. David, R. Bhandavat, U. Barrera and G. Singh, *Nat. Commun.*, 2016, **7**, 10998–11007.

13 T. Gao, Q. T. Qu, G. B. Zhu, Q. Shi, F. Qian, J. Shao and H. H. Zheng, *Carbon*, 2016, **110**, 249–256.

14 J. W. Zhou and B. Wang, *Chem. Soc. Rev.*, 2017, **46**, 6927–6945.

15 Y. Lin, Q. Zhang, C. Zhao, H. Li, C. Kong, C. Shen and L. Chen, *Chem. Commun.*, 2015, **51**, 697–699.

16 T. An, Y. Wang, J. Tang, Y. Wang, L. Zhang and G. Zheng, *J. Colloid Interface Sci.*, 2015, **445**, 320–325.

17 H. Furukawa, N. Ko, Y. B. Go, N. Aratani, S. B. Choi, E. Choi, A. Ö. Yazaydin, R. Q. Snurr, M. O'Keeffe, J. Kim and O. M. Yaghi, *Science*, 2010, **329**, 424–428.

18 E. D. Bloch, W. L. Queen, R. Krishna, J. M. Zadrozny, C. M. Brown and J. R. Long, *Science*, 2012, **335**, 1606–1610.

19 C. Wang, T. Zhang and W. Lin, *Chem. Rev.*, 2012, **112**, 1084–1104.

20 W. Li, J. Liu and D. Zhao, *Nat. Rev. Mater.*, 2016, **1**, 16023–16039.

21 T. Yamada, K. Shiraishi, H. Kitagawa and N. Kimizuka, *Chem. Commun.*, 2017, **53**, 8215–8218.

22 G. Férey, F. Millange, M. Morcrette, C. Serre, M. Doublet, J. Grenèche and J. Tarascon, *Angew. Chem., Int. Ed.*, 2007, **46**, 3259–3263.

23 D. H. Yang, X. Zhou, M. Zhong, Z. Zhou and X. H. Bu, *ChemNanoMat*, 2017, **3**, 252–258.

24 K. J. Lee, T.-H. Kim, T. K. Kim, J. H. Lee, H.-K. Song and H. R. Moon, *J. Mater. Chem. A*, 2014, **2**, 14393–14400.

25 F. Zhang, D.-D. Qi and X.-G. Zhang, *Int. J. Electrochem. Sci.*, 2016, **11**, 189–199.

26 W. Xu, X. Cui, Z. Xie, G. Dietrich and Y. Wang, *Electrochim. Acta*, 2016, **222**, 1021–1028.

27 R. Wu, X. Qian, X. Rui, H. Liu, B. Yadian, K. Zhou, J. Wei, Q. Yan, X.-Q. Feng, Y. Long, L. Wang and Y. Huang, *Small*, 2014, **10**, 1932–1938.

28 H. Li, Y. Su, W. W. Sun and Y. Wang, *Adv. Funct. Mater.*, 2016, **26**, 8345–8353.

29 R. Sibille, T. Mazet, B. Malaman, Q. Wang, E. Didelot and M. François, *Chem. Mater.*, 2015, **27**, 133–140.

30 Y. Jiao, J. Pei, D. Chen, C. S. Yan, Y. Y. Hu, Q. Zhang and G. Chen, *J. Mater. Chem. A*, 2017, **5**, 1094–1102.

31 Y. P. He, Y. X. Tan and J. Zhang, *J. Mater. Chem. C*, 2014, **2**, 4436–4441.

32 H. R. Fu, Z. X. Xu and J. Zhang, *Chem. Mater.*, 2015, **27**, 205–210.

33 S. Das, H. Kim and K. Kim, *J. Am. Chem. Soc.*, 2009, **131**, 3814–3815.

34 D. J. Tranchemontagne, J. L. Mendoza-Cortés, M. O'Keeffe and O. M. Yaghi, *Chem. Soc. Rev.*, 2009, **38**, 1257–1283.

35 L. Li, S. L. Xiang, S. Q. Cao, J. Y. Zhang, G. F. Ouyang, L. P. Chen and C. Y. Su, *Nat. Commun.*, 2013, **4**, 1774–1782.

36 D. W. Feng, K. C. Wang, Z. W. Wei, Y. P. Chen, C. M. Simon, R. K. Arvapally, R. L. Martin, M. Bosch, T. F. Liu, S. Fordham, D. Q. Yuan, M. A. Omary, M. Haranczyk, B. Smit and H. C. Zhou, *Nat. Commun.*, 2014, **5**, 5723–5730.

37 Y. Zhu, X. Fan, L. Suo, C. Luo, T. Gao and C. Wang, *ACS Nano*, 2016, **10**, 1529–1538.

38 H. Tang, S. Yao, M. Jing, X. Wu, J. Hou, X. Qian, D. Rao, X. Shen, X. Xi and K. Xiao, *Electrochim. Acta*, 2015, **176**, 442–447.

39 Y. P. Du, Z. Y. Yin, J. X. Zhu, X. Huang, X. J. Wu, Z. Y. Zeng, Q. Y. Yan and H. Zhang, *Nat. Commun.*, 2012, **3**, 1177–1183.

40 B. Jache, B. Mogwitz, F. Klein and P. Adelhelm, *J. Power Sources*, 2014, **247**, 703–711.

41 A. B. Blake, A. Yavari, W. E. Hatfield and C. N. Sethulekshmi, *J. Chem. Soc., Dalton Trans.*, 1985, **12**, 2509–2520.

42 G. M. Sheldrick, *SADABS; ver. 2.10*, University of Gottingen, Göttingen, Germany, 2003.

43 G. M. Sheldrick, *SHELX-97, Program for Crystal Structure Refinement*, University of Göttingen, Germany, 1997.

44 A. Schoedel and M. Zaworotko, *J. Chem. Sci.*, 2014, **5**, 1269–1282.

45 I. D. Brown and D. Altermatt, *Acta Crystallogr., Sect. B: Struct. Sci.*, 1985, **41**, 244–247.

46 N. E. Brese and M. O'Keeffe, *Acta Crystallogr., Sect. B: Struct. Sci.*, 1991, **47**, 192–197.

47 A. L. Spek, *PLATON: A Multipurpose Crystallographic Tool*, Utrecht University, Utrecht, The Netherlands, 1999.

48 R. Fong, U. Sacken and J. R. Dahn, *J. Electrochem. Soc.*, 1990, **137**, 2009–2013.